PERFORMANCE OF ROOT-MUSIC ALGORITHM USING REAL-WORLD ARRAYS

Fabio Belloni, Andreas Richter, and Visa Koivunen

Signal Processing Laboratory, SMARAD CoE, Helsinki University of Technology (HUT)
Otakaari 5A, 02150, Espoo, Finland
phone: +(358) 9451 2407, fax: +(358) 9452 3614, email: {fbelloni,arichter,visa}@wooster.hut.fi
web: wooster.hut.fi

ABSTRACT

In this paper we study the performance of the root-MUSIC algorithm and its extensions to non-ULA configurations using real-world antenna arrays. These arrays are non-ideal and built using directional elements, where each sensor has its own directional beampattern. We describe the Element-Space (ES) root-MUSIC algorithm for Direction-of-Arrival (DoA) estimation [1]. It uses the manifold separation technique and allows extending the known root-MUSIC algorithm to non-ULA configurations. We explain how to select the number of modes in order to minimize the array modelling error, when applying the manifold separation technique. Finally, we evaluate the ES-root-MUSIC algorithm using real-world antenna array data. The simulation results demonstrate that statistical performance close to the Cramér-Rao Bound is obtained using real-world arrays with all their imperfections.

1. INTRODUCTION

In array signal processing it is often convenient to work with arrays having a steering vector matrix with a Vandermonde structure. For example, this allows using rooting-based Direction-of-Arrival (DoA) estimation algorithms having a low computational complexity, such as root-MUSIC and root-WSF [3]. Originally, these algorithm were designed for ideal Uniform Linear Arrays (ULA). Later, techniques known as array interpolation [2] and beamspace transform [3]-[4] have been developed in order to map the steering vectors of a planar array onto steering vectors of a ULA-type array, called the virtual array. These preprocessing techniques often introduce mapping errors in the form of bias and excess variance [4]. This leads to DoA estimates which are not statistically efficient.

Recently, we have proposed an algorithm called Element-Space (ES) root-MUSIC [1], which provides 1-D (azimuth only) DoA estimation of non-coherent sources. The ES-root-MUSIC algorithm has low computational complexity, and processes the data recorded by the array directly in element-space. Hence, no transformation or interpolation of the data is required, and mapping error can be avoided. Instead, it uses a convenient remodelling of the antenna arrays steering vector for performing fast (search-free) DoA estimation on arbitrary array configurations.

In this paper, we have considered five real-world antenna arrays with different configurations in order to test both the applicability and the robustness of the ES-root-MUSIC algorithm [1]. The algorithm can handle arbitrary array configurations since it jointly exploits the concept of manifold separation [1]-[7] and Effective Aperture Distribution Function (EADF) [8]-[9]. The EADF can be expressed by the IDFT (Inverse Discrete Fourier Transform) of calibration measurements and it represents a sufficiently accurate description of the real-world array including array imperfections. The calibration measurements, used to compute the array model, contain array non-idealities, such as mutual coupling between sensors, antenna manufacturing errors, sensors orientation and position. By simulation results, we show that the ES-root-MUSIC is robust to array imperfections and it can be applied to arrays with both directional or omnidirectional sensors.

This paper is organized as follows. First, the models for real-world antenna arrays, and the employed signal model are presented.

In Section 3, we introduce the antenna arrays used for performance evaluation. In Section 4, we give a brief overview of the ES-root-MUSIC algorithm [1]. A way to compute an approximation of the CRB (Cramèr-Rao Bound) for real-world arrays is also presented here. In Section 5, we show the simulation results by means of the statistical performance of ES-root-MUSIC when applied to real-world arrays. Finally, Section 6 concludes the paper.

2. MODELLING OF REAL-WORLD ARRAYS

Let us have an array of N sensors, where every element has an individual directional characteristic. We define the origin of the coordinate system to be at the centroid of the array. The co-elevation angle θ is measured down from the z-axis (assumed to be fixed at $\theta = 90°$) and ϕ is the azimuth angle measured counterclockwise from the x-axis in the xy-plane. The array steering vector of an arbitrary antenna array can be expressed using the concepts of manifold separation and EADF [1],[6]-[9].

The response of an antenna array to a far field source can be modeled by measuring the directional characteristic of the antenna in an anechoic chamber. For our purposes, we may measure the array response to a far field source by moving the source around the array at a fixed co-elevation angle $\theta = 90°$ along the azimuthal direction in the range $\phi \in [-\pi, \pi)$. Alternatively, the same result can be obtained by measuring the antenna by rotating the array about its centroid. This creates a discrete set of measured points (along the direction ϕ), which represents a discrete periodic function with period 2π in azimuth. Hence, the beampattern of the n-th sensor within the array can be expressed by an IDFT (Inverse Discrete Fourier Transform) of the measured data (calibration data). We will refer to this as Effective Aperture Distribution Function (EADF).

It is important to notice that the characteristic of each sensor is measured by considering the whole antenna array. Consequently, the measured beampattern of each sensor contains the influence of all elements in the antenna array.

By using the transformed array calibration measurement (EADF) and the concept of manifold separation, we can define the beampattern of the n-th sensor $b_n(\phi)$ of a real-world array as

$$b_n(\phi) = \mathbf{g}_n \mathbf{d}(\phi) + \mathcal{O}(\mathcal{M}) , \qquad (1)$$

where $\mathbf{g}_n \in \mathbb{C}^{1 \times \mathcal{M}}$ is the characteristic vector (EADF) of the n-th sensor and $\mathbf{d}(\phi) \in \mathbb{C}^{\mathcal{M} \times 1}$ is the Vandermonde structured vector

$$\mathbf{d}(\phi) = \frac{1}{\sqrt{\mathcal{M}}} \left[e^{-j\frac{\mathcal{M}-1}{2}\phi}, \dots, e^{-j\phi}, 1, e^{j\phi}, \dots, e^{j\frac{\mathcal{M}-1}{2}\phi} \right]^T . \quad (2)$$

In practice, the EADF vector $\mathbf{g}_n$ is computed using the IDFT of the array calibration measurements. Here, $\mathcal{M}$ denotes the number of modes and $\mathcal{O}(\mathcal{M})$ represents a modelling error, which may be made infinitesimally small by increasing $\mathcal{M}$. For details about the selection of $\mathcal{M}$, see Section 2.1.

In real-world antenna arrays, every sensor has a unique beampattern, which is influenced by the neighboring sensors (mutual coupling). As depicted in Fig. 1, the EADF of each sensor is different from the other ones. Since the EADF is determined from
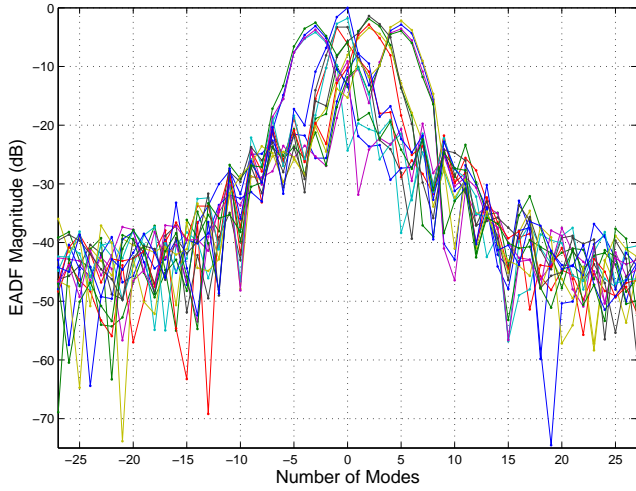
Figure 1: EADFs computed from the calibration data of the URPA, which is described in section 3. Each line defines the characteristic function of one of the sensors in the array. Due to its specific beampattern and mutual coupling, each element is described by a different EADF.

Figure 2: Ideal and real-world EADFs computed from $Q = 360$ simulated and calibration points, respectively. The measurement noise level σ_w^2 limits the maximum number of eligible modes $\mathcal{M}$. The truncated EADF is within the truncation boundaries.

array calibration measurement, we can state that the EADF represents a sufficiently accurate description of the array. A comparison between the EADFs of an ideal and a real-world array can be found in [5].

The manifold separation technique expressed in eq. (1) has an useful property. It is easy to differentiate. In fact, since the characteristic vector $\mathbf{g}_n$ is independent from the unknown angular parameter ϕ [7], the derivative of the n-th sensor beampattern with respect to ϕ can simply be expressed as [8],[9]

$$\delta_n(\phi) = \frac{\partial b_n(\phi)}{\partial \phi} = \mathbf{g}_n \frac{\partial \mathbf{d}(\phi)}{\partial \phi} \ . \tag{3}$$

Equation (3) is exploited in Section 4.1 for deriving the CRB of practical antenna arrays.

2.1 Selection of the Number of Modes

The selection of the number of modes $\mathcal{M}$ in $\mathbf{g}_n$, eq. (1), is a critical step in modelling an antenna array, because this controls the modelling error $\mathcal{O}(\mathcal{M})$. Observe that due to the structure of the Vandermonde vector $\mathbf{d}(\phi)$, $\mathcal{M}$ is an odd number.

As described in [1], in case of an ideal array, the number of modes may by chosen such that the modelling error $\mathcal{O}(\mathcal{M})$ becomes arbitrary small. Hence, we can choose the number of modes in the range $N \leq \mathcal{M} \leq Q$, where Q is the number of calibration angles. On the other hand, by using real-world calibration data, we have an upper bound for selecting the number of modes. This limit is given by the error floor in the computed real-world EADF, which is mainly determined by the noise in the calibration measurements. Consequently, we have a smaller selection range $N \leq \mathcal{M} \leq \mathcal{M}_\eta \leq Q$, where $|m| = (\mathcal{M}_\eta - 1)/2$ is the index of the highest mode having a magnitude larger than the calibration noise standard deviation σ_w.

In Fig. 2, we depict an example of EADF computed by using both synthetical and measured calibration data. The plot represents the EADF of a sensor in the array. We can see from the picture that the modes with a magnitude larger than the measurement noise level are similar in the ideal and real-world case. When calibration measurements are used, the computed EADF saturates at the measurement error level, while for simulated data the saturation point is given by the computational accuracy of the used machine (e.g. IEEE-754, 64 bit float ~ 310 dB). As a result, the number of modes
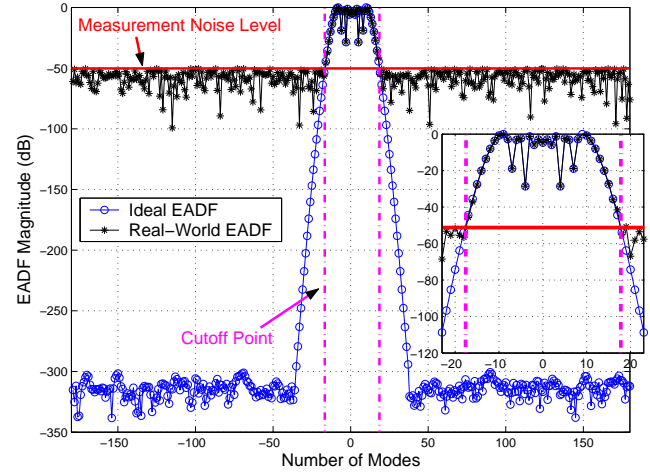
$\mathcal{M}$ is given by the number of modes having magnitude larger than the calibration measurements noise, i.e. $\mathcal{M} = \mathcal{M}_\eta$.

Generally, the model of the antenna array will contain modelling errors, which are proportional to the measurement noise variance σ_w^2 in the EADF. This error affects the performance of ES-root-MUSIC by introducing a systematic error (bias) in the estimates. However, it is important to remember that in a real-world radio system, the SNR is limited by the available transmit power and the receiver noise. Consequently, whenever the SNR $\ll \min_\phi(\|\mathbf{b}(\phi)\|)/\mathcal{O}(\mathcal{M})$, the residual modelling error can be neglected and eq. (1) still holds. In other words, if the bias created by $\mathcal{O}(\mathcal{M})$ is smaller than the variance of the DoA estimates at the highest achievable SNR, the bias in the DoA estimates can be neglected because it is still significantly smaller than the variance of the estimates.

The selection of the number of modes also defines the cutoff points of the EADF, see Fig. 2. The truncation of the EADF has two main effects. First, it reduces the amount of data that we have to store [8]. Second, truncating the EADF improves the accuracy of the array data model by a factor of $\sim 10 \log_{10}(Q/\mathcal{M})$ in SNR. This is an improvement compared to algorithms working directly with the calibration measurements.

2.2 Signal Model

We assume that there are P $(P < N)$ non-coherent narrowband signal sources on the xy-plane, impinging the array from directions $\phi = \{\phi_1, \ldots, \phi_P\}$, where ϕ is the azimuth angle. Furthermore, we assume that K snapshots are observed by the array. The array output matrix $\mathbf{X} \in \mathbb{C}^{N \times K}$ may be written as

$$\mathbf{X} = \mathbf{BS} + \mathbf{N}, \tag{4}$$

where $\mathbf{B} = [\mathbf{b}(\phi_1), \mathbf{b}(\phi_2), \ldots, \mathbf{b}(\phi_P)] \in \mathbb{C}^{N \times P}$, with $\mathbf{b}(\phi_p) = [b_0(\phi_p), b_1(\phi_p), \ldots, b_{N-1}(\phi_p)]^T \in \mathbb{C}^{N \times 1}$, is the array steering vector matrix, $\mathbf{S} \in \mathbb{C}^{P \times K}$ is the signal matrix with rank$(\mathbf{SS}^H) = P$ and $\mathbf{N} \in \mathbb{C}^{N \times K}$ contains the observation noise. The noise is modelled as a stationary, second-order ergodic, zero-mean, spatially and temporally, white circular complex Gaussian process.

Figure 3: Polarimetric Uniform Linear Patch Array (PULPA) with $N = 8$ patch sensors (TU-Ilmenau).

Figure 4: On the LHS, Polarimetric Uniform Circular Patch Array (PUCPA) with $N = 24$ patch elements. On the RHS, Stack Polarimetric Uniform Circular Patch Array (SPUCPA) with $N = 24$ patch sensors. Courtesy of TU-Ilmenau.
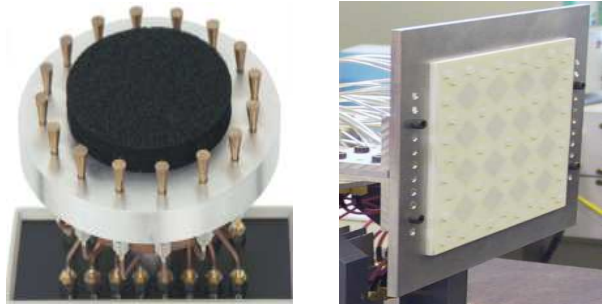
Figure 5: On the LHS, Uniform Circular Array (UCA) with $N = 16$ conical sensors (TU-Ilmenau). On the RHS, Uniform Rectangular Polarimetric Array (URPA) with $N = 16$ patch elements (HUT).

Figure 6: Statistical performance of ES-root-MUSIC when used on the PULA with $N = 8$ sensors and $\mathcal{M} = 55$ selected modes.

3. REAL-WORLD ANTENNA ARRAYS

In this section, the five real-world antenna arrays which have been used for experimental results are described. The antennas were designed for a center frequency $f_0 \in [5.2, 5.4]$ GHz and have a bandwidth of 120 MHz [8],[10]. The following four arrays were provided by the Electronic Measurement Research Laboratory, TU-Ilmenau, Germany.

In Fig 3, a Polarimetric Uniform Linear Patch Array (PULPA) is depicted. This antenna has $N = 8$ patch sensors with a interelement spacing $d = 0.4943\lambda$. Each element has one port for horizontal and one port for vertical polarization.

In Fig. 4 (left), we show the $N = 24$ elements Polarimetric Uniform Circular Patch Array (PUCPA) and (right) the $N = 96$ elements Stack Polarimetric Uniform Circular Patch Array (SPUCPA). The SPUCPA is comprised of 4 stacked rings of 24 polarimetric patches. It has 192 output ports in total. The switch is arranged inside the cylinder [8],[9].

On the left hand side of Fig. 5, the Uniform Circular Array (UCA) with $N = 16$ conical elements is depicted. Examples of sensors beampattern for this antenna array can be found in [5].

Finally, on the right hand side of Fig. 5, we show the Uniform Rectangular Patch Array (URPA) with $N = 16$ polarimetric patch elements. The antenna was provided by the Radio Laboratory, SMARAD CoE, Helsinki Univ. of Technology (HUT), Finland.

The goal of this paper is to study the statistical performance of the recently proposed ES-root-MUSIC algorithm [1] using these five real-world antenna arrays. As we will see in Section 5, this DoA estimation algorithm can be applied to different array configurations, and it achieves statistical performance close to the CRB.

4. ELEMENT-SPACE ROOT-MUSIC

Here we briefly present the ES-root-MUSIC algorithm. For more details, see [1]. In particular, we focus on the advantages given by this algorithm for implementation on real-world systems.

In order to remodel the steering vector of an arbitrary array, the ES-root-MUSIC algorithm exploits the manifold separation technique [1],[6],[7]. In this way, the array steering vector can be expressed as the product of the characteristic array matrix (EADF) and a vector with a Vandermonde structure containing the unknown parameter. The ES-root-MUSIC allows azimuthal DoA estimation of non-coherent sources at a fixed elevation angle.
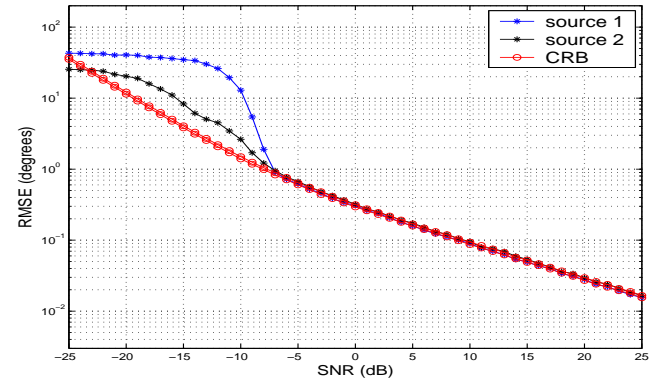
Combining eq. (1) and (4), we can rewrite the system model as

$$\mathbf{X} = \mathbf{B}\mathbf{S} + \mathbf{N} = \mathbf{G}\mathbf{D}\mathbf{S} + \mathbf{N} \,, \tag{5}$$

where $\mathbf{D} \in \mathbb{C}^{\mathcal{M} \times P}$ is a matrix formed as $\mathbf{D} = [\mathbf{d}(\phi_1), \dots, \mathbf{d}(\phi_P)]$, and $\phi_1, \dots, \phi_P$ are the true DoAs of the P non-coherent sources. Here, $\mathbf{G} \in \mathbb{C}^{N \times \mathcal{M}}$ is the EADF matrix (characteristic matrix of the array) defined as

$$\mathbf{G} = [\mathbf{g}_0, \mathbf{g}_1, \dots, \mathbf{g}_{N-1}]^T, \tag{6}$$

where $\mathbf{g}_n \in \mathbb{C}^{1 \times \mathcal{M}}$ $(n = 0, \dots, N-1)$ is the EADF vector of the n-th array sensor, computed by selecting the $\mathcal{M}$ modes of the IDFT of the calibration measurements [1],[8],[9], see Section 2.1.

The element-space array covariance matrix can be expressed by

$$\mathbf{R}_x = \mathbf{E}_s \mathbf{\Lambda}_s \mathbf{E}_s^H + \sigma_\eta^2 \mathbf{E}_\eta \mathbf{E}_\eta^H = \mathbf{G}\mathbf{D}\mathbf{R}_s \mathbf{D}^H \mathbf{G}^H + \sigma_\eta^2 \mathbf{I} \,, \tag{7}$$

where $\mathbf{I}$ is the $N \times N$ identity matrix, $\mathbf{R}_s$ is the $P \times P$ signal covariance matrix, and $\mathbf{E}_s$ and $\mathbf{E}_\eta$ span the $N \times P$ signal and the $N \times (N-P)$ noise subspaces, respectively. The key idea used in the derivation of the ES-root-MUSIC algorithm is that $\mathbf{E}_s$, $\mathbf{B}$ and $\mathbf{G}\mathbf{D}$ span the same subspace. Consequently, $\mathbf{G}\mathbf{D}$ is orthogonal to the noise subspace $\mathbf{E}_\eta$ [1].

Therefore, for a real-world array of arbitrary configuration, we can express the pseudo-spectrum of the ES-MUSIC algorithm as [1]

$$S_{music}(\phi) = \left(\mathbf{d}^H(\phi)\mathbf{G}^H \mathbf{E}_\eta \mathbf{E}_\eta^H \mathbf{G}\mathbf{d}(\phi)\right)^{-1} \,, \tag{8}$$

which allows applying fast (search-free) polynomial rooting algorithms (e.g. root-MUSIC). By substituting $z = e^{j\phi}$ into the $\mathcal{M} \times 1$ Vandermonde structured vector $\mathbf{d}(\phi)$, eq. (8) can be rewritten in polynomial form. Hence the phase angles of the P roots closest to the unit circle, z_p, will yield the azimuth estimates, $\widehat{\phi}_p = \angle(z_p)$, of sources at a given elevation angle.

For practical systems, the proposed ES-root-MUSIC algorithm has three main advantages over the conventional MUSIC technique implemented by using only the measured elements beampattern. First, by transforming the measured beampattern from the angular to the modal domain (EADF), we benefit from the SNR gain described in Section 2.1. Second, by using the compressed information contained in the EADF, we effectively reduce the data required for modelling the antenna array [8],[9]. In fact, only a relatively small number of modes $\mathcal{M}$ of the EADF are sufficient for accurately describing the array. Last, but not least, by combining manifold separation and EADF we can perform search-free DoA estimation by processing the data directly in the element-space domain using well known rooting-based techniques, e.g. root-MUSIC. The necessary steps to perform DoA estimation using arbitrary arrays and root-MUSIC are summarized in Table 1.

Table 1: Element-Space root-MUSIC

- Offline processing steps:
    1. Acquire calibration measurements of the array at the highest possible SNR with a high angular resolution, i.e. choose a large Q.
    2. Compute the EADFs from the calibration measurements using the IDFT.
    3. Truncate the EADFs and form $\mathbf{G}$ in equation (6).
- Perform angular estimation (online processing):
    1. Form the element-space array data matrix $\mathbf{X}$.
    2. Compute the noise subspace (element-space) $\mathbf{E}_\eta$ as in eq. (7).
    3. Use the standard root-MUSIC implementation on eq. (8) to estimate the DOAs.

4.1 CRB for Real-World Arrays

In this section, we derive an approximate CRB used for comparing and evaluating the statistical performance of the ES-root-MUSIC algorithm when applied to different practical antenna array configurations.

It is important to note that the following derivation gives the exact CRB for the array model, in eq. (5), used in the implementation of the ES-root-MUSIC algorithm, but only an approximation of the exact CRB for a given antenna array. This is due to the modelling error in eq. (1), which can be made small only up to a threshold that depends on the measurement noise σ_w^2 in the calibration data, see Section 2.1. However, if the calibration measurements are properly done, the modelling error can be neglected and the approximated CRB still describes the performance bounds (at the highest possible SNR) of a given real-world array with sufficient accuracy.

The signals in $\mathbf{S}$ used in our simulations are stochastic signals. Consequently, we use the stochastic CRB as a performance measure for the proposed algorithm. The stochastic CRB is defined as the inverse of the Fisher Information Matrix (FIM). This matrix gives the relative rate (derivative) at which the probability density function of the estimator changes with respect to data (curvature of the log-likelihood function) [9],[11]. By combining the derivation property of the manifold separation, eq. (3), and using the result in [11], we find the CRB (as a function of the incident angles ϕ) as

$$\text{CRB}(\phi) = \frac{\sigma_\eta^2}{2K} \left\{ \Re\left[(\boldsymbol{\Delta}^H \boldsymbol{\Pi}_\eta \boldsymbol{\Delta}) \odot (\mathbf{R}_s \mathbf{B}^H \mathbf{R}_x^{-1} \mathbf{B} \mathbf{R}_s)^T \right] \right\}^{-1}, \tag{9}$$

where $\boldsymbol{\Delta} = [\boldsymbol{\delta}_1, \ldots, \boldsymbol{\delta}_P]$ with

$$\boldsymbol{\delta}_p = \left.\frac{\partial \mathbf{b}(\phi)}{\partial \phi}\right|_{\phi=\phi_p} = \mathbf{G} \left.\frac{\partial \mathbf{d}(\phi)}{\partial \phi}\right|_{\phi=\phi_p}. \tag{10}$$

Here, $\boldsymbol{\delta}_p \in \mathbb{C}^{N \times 1}$ contains the derivative of the array steering vector with respect to the angle ϕ, evaluated at a certain DoA, $\mathbf{B}$ is the $N \times P$ array steering matrix, $\mathbf{R}_s$ is the $P \times P$ signal covariance matrix, $\mathbf{R}_x$ is the $N \times N$ array covariance matrix, K is the number of snapshots, σ_η^2 is the AWGN power and $\odot$ denotes the Hadamard-Schur product, i.e., element-wise multiplication. Moreover, $\boldsymbol{\Pi}_\eta = \mathbf{I} - \boldsymbol{\Pi}_s$ and $\boldsymbol{\Pi}_s = \mathbf{B}(\mathbf{B}^H \mathbf{B})^{-1} \mathbf{B}^H$ are the $N \times N$ projection matrices to noise subspace and to signal subspace, respectively.

It is well known that, in the low SNR region, this CRB is not the proper bound for DoA estimation algorithms. For example, in the very low SNR region of Fig. 6, the CRB is not valid. This is due to the fact that the information about the limited support of the angle to estimate is not used in the derivation of the CRB, i.e $\phi \in (-\frac{\pi}{2}, \frac{\pi}{2})$ for a ULA. On the other hand, this region is not of practical interest.

5. SIMULATION RESULTS

Here, we present simulation results showing the statistical performance of the ES-root-MUSIC algorithm when used on non-ideal real-world arrays with different configurations. For the performance evaluation of the algorithm, we focus on the middle/high SNR region, i.e. when the CRB becomes the proper lower bound.

For the simulations, the following settings have been used: two uncorrelated sources impinging the arrays from the azimuth angles $(\phi_1, \phi_2) = (25°, 35°)$, $K = 256$ recorded snapshots and 2000 independent Monte Carlo trials.

Note that since the characteristic matrix (EADF) $\mathbf{G}$ of each array has been computed by using real-world calibration data, we have normalized the recorded data $\mathbf{X}$ by a factor $\|\mathbf{G}\|_F / \sqrt{N\mathcal{M}}$. This factor scales the recorded data in order to normalize the power received either by a single sensor than by the entire antenna array. In other words, the power received by a sensor is normalized by its average received power, as well as the total power received by the array (considering all the sensors) is normalized by the average power among all the sensors. Note that the normalization factor fixes the average array gain of the antenna arrays over the interval $[-\pi, \pi)$ to N, i.e. the number of sensors.

As a result, by using the aforementioned normalization factor, we can now compare the performance limits (CRB) of the five different real-world array configurations.

In Fig. 8, we give the performance of the $N = 24$ elements PUCPA, while Fig. 9 shows the performance of the $N = 96$ elements SPUCPA. The aperture of the arrays in azimuth is equivalent. Consequently, the CRB should differ by the array gain only, which is $10 \log_{10}(96/24) \simeq 6$ dB.

Throughout Fig. 6-10 we can clearly see that the ES-root-MUSIC algorithm [1] has close to optimal performance for all five real-world array configurations. The algorithm also appears to be robust with respect to antenna non-idealities. The statistical performance of ES-root-MUSIC is close to the respective CRB and has a consistent behavior in all the analyzed scenarios.

6. CONCLUSIONS

In this paper, we studied the statistical performance of the Element-Space (ES) root-MUSIC algorithm. The selection of the number of modes, when real-world antenna arrays are used, is also discussed.

The calibration measurements, used to compute the array model, contain array non-idealities such as mutual coupling between sensors, antenna manufacturing errors and, sensors orientation and position.

An approximate stochastic CRB for practical arrays has been derived. Simulation results show that ES-root-MUSIC algorithm can perform 1-D (azimuth only) DoA estimation at a fixed elevation
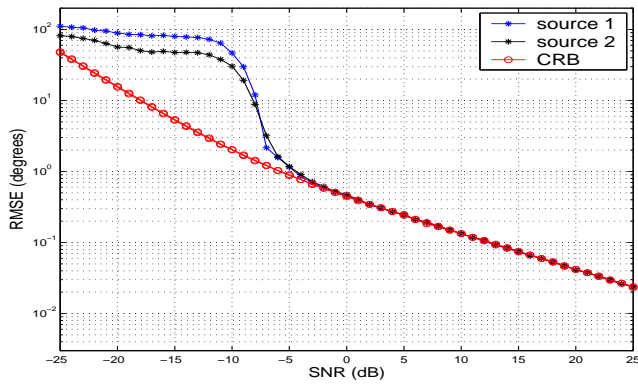
Figure 7: Statistical performance of ES-root-MUSIC when used on the UCA with $N = 16$ sensors and $\mathcal{M} = 25$ selected modes.
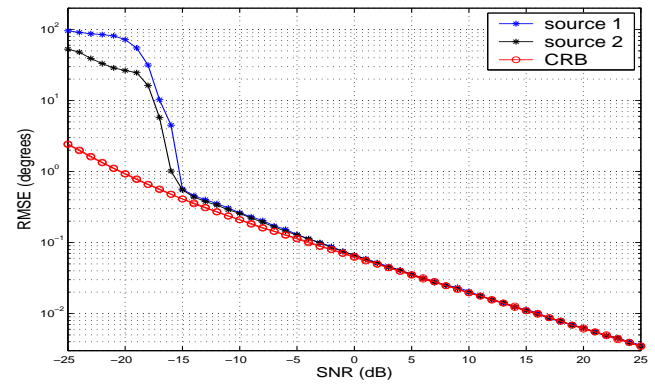
Figure 9: Statistical performance of ES-root-MUSIC when used on the SPUCPA with $N = 96$ sensors and $\mathcal{M} = 41$ selected modes.
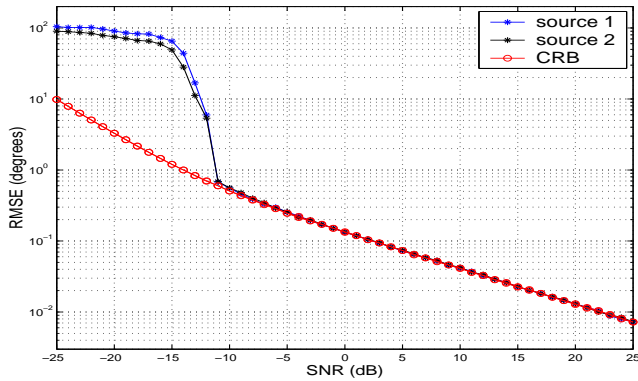
Figure 8: Statistical performance of ES-root-MUSIC when used on the PUCPA with $N = 24$ sensors and $\mathcal{M} = 45$ selected modes.
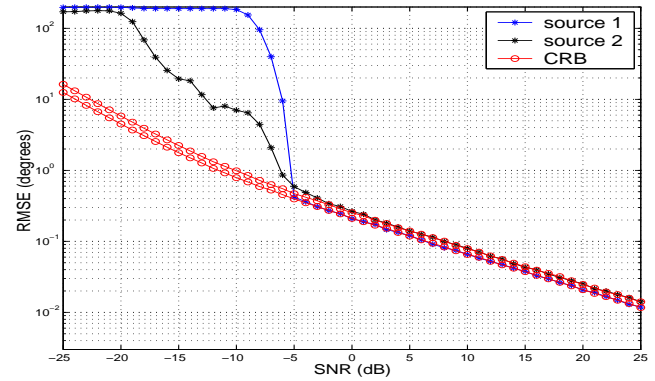
Figure 10: Statistical performance of ES-root-MUSIC when used on the URPA with $N = 16$ sensors and $\mathcal{M} = 55$ selected modes.

angle on arbitrary array configurations. The algorithm performance is close to the CRB regardless of the array imperfections.

7. ACKNOWLEDGEMENTS

REFERENCES

[1] Belloni, F.; Richter, A.; Koivunen, V.; *Extension of root-MUSIC to non-ULA Array Configurations*, Proc. of the IEEE International Conference on Acoustics, Speech, and Signal Processing (ICASSP), France, May 14-19, 2006.

[2] Buhren, M.; Pesavento, M.; Böhme, J.F.; *Virtual array design for array interpolation using differential geometry*. Proc. of IEEE International Conference on Acoustics, Speech, and Signal Processing (ICASSP), Vol. 2, May 2004, pp: 229-232.

[3] Lau, B.K.; *Applications of Antenna Arrays in Third-Generation Mobile Communications*. Ph.D. Thesis, Curtin University of Technology, Perth, Australia, 2002.

[4] Belloni, F.; Koivunen, V.; *Beamspace Transform for UCA: Error Analysis and Bias Reduction*, Technical Report No. 48, ISBN: 951-22-7292-X, Signal Processing Laboratory, Helsinki Univ. of Technology, 2004 (To appear in the IEEE Tr. on Signal Processing, Accepted for publication in Sept. 2005).

[5] Belloni, F.; Richter, A.; Koivunen, V.; *"Avoiding Bias in Circular Arrays Using Optimal Beampattern Shaping and EADF*, Proc. of the 39-th Annual Asilomar Conference on Signals, Systems and Computers, Pacific Grove, California, Oct. 30-Nov. 2, 2005.

[6] Doron, M.A.; Doron, E.; Weiss, A.J.; *Coherent Wide-Band Processing for Arbitrary Array Geometry*. IEEE Tr. Signal Processing, Vol. 41, Issue 1, January 1993, Page(s):414-417.

[7] Doron, M.A.; Doron, E.; *Wavefield modeling and array processing .I. Spatial sampling*, IEEE Tr. Signal Processing, Vol. 42, Issue 10, Oct. 1994, Page(s): 2549-2559.

[8] Thoma, R.S.; Landmann, M.; Sommerkorn, G.; Richter, A.; *Multidimensional high-resolution channel sounding in mobile radio*. Proc. of the 21-st IEEE Instrumentation and Measurement Technology Conference (IMTC), Vol. 1, 18-20 May 2004, Page(s): 257-262.

[9] Richter, A.; *Estimation of Radio Channel Parameters: Models and Algorithms*. Ph.D. Thesis Dissertation, Technische Universität Ilmenau, Ilmenau, Germany, 2005, ISBN 3-938843-02-0, urn:nbn:de:gbv:ilm1-2005000111, Online: www.db-thueringen.de.

[10] Kolmonen, V.-M.; Kivinen, J.; Vuokko, L.; Vainikainen, P.; *5.3 GHz MIMO radio channel sounder*, Intrumentation and Measurement Technology Conference (IMTC), Vol. 3, Ottawa, Canada, 17-19 May 2005, Page(s): 1883-1888.

[11] Stoica, P.; Larsson, E.G.; Gershman, A.B.; *The stochastic CRB for array processing: a textbook derivation*. IEEE Signal Processing Letters, Vol. 8 Issue: 5, May 2001, pp: 148-150.